Minimum entropy generation in a heat exchanger in the cryogenic part of the hydrogen liquefaction process: On the validity of equipartition and disappearance of the highway

Ragnhild Hånde [a], Øivind Wilhelmsen [b,c,]*

[a] *NTNU, Department of Physics, NO-7491 Trondheim, Norway*
[b] *NTNU, Department of Energy and Process Engineering, NO-7491 Trondheim, Norway*
[c] *SINTEF Energy Research, Sem Sælands vei 11, NO-7034 Trondheim, Norway*

ARTICLE INFO

ABSTRACT

Liquefaction of hydrogen is a promising technology for transporting large quantities of hydrogen across long distances. A key challenge is the high power consumption. In this work, we discuss refrigeration strategies that give minimum entropy production/exergy destruction in a plate-fin heat exchanger that cools the hydrogen from 47.8 K to 29.3 K. Two reference cases are studied; one where the feed stream enters at 20 bar, and one where it enters at 80 bar. Catalyst in the hot layers speeds up the conversion of ortho-to para-hydrogen. Optimal control theory is used to formulate a minimization problem where the objective function is the total entropy production, the control variable is the temperature of the refrigerant and the constrains are the balance equations for energy, mass and momentum in the hot layers. The optimal refrigeration strategies give a reduction of the total entropy production of 8.7% in the 20-bar case and 4.3% in the 80-bar case. The overall heat transfer coefficient and duty is higher in the 20 bar case, which compensates for the increase in entropy production due to a thermal mismatch that is avoided in the 80 bar case. This leads the second law efficiency of the 20 bar case (91%) to be similar to the 80 bar case (89%). We demonstrate that equipartition of the entropy production and equipartition of the thermal driving force are both excellent design principles for the process unit considered, with total entropy productions deviating only 0.2% and 0.5% from the state of minimum entropy production. Equipartition of the thermal driving force i.e. a constant difference between the inverse temperatures of the hot and cold layers represents a particularly simple guideline that works remarkably well. We find that both heat transfer and the spin-isomer reaction contribute significantly to the entropy production throughout the length of the process unit. Unlike previous examples in the literature, the process unit considered in this work is not characterized by a "reaction mode" at the inlet followed by a "heat transfer mode". Therefore, it does not follow a highway in state space, i.e. a band that is particularly dense with energy efficient solutions. By artificially increasing the spin-isomer conversion rate, the highway appears when the conversion rate becomes sufficiently high.

© 2019 The Authors. Published by Elsevier Ltd on behalf of Hydrogen Energy Publications LLC. This is an open access article under the CC BY license (http://creativecommons.org/licenses/by/4.0/).

Introduction

A major challenge in a future mass deployment scenario of hydrogen as an energy carrier is energy- and cost-efficient transport and distribution from production sites to end users. Preferred transport and distribution of the hydrogen has analogies with that of natural gas, where large quantities and short distances favor pipeline transport, lower quantities and short distances point towards compressed hydrogen, and large quantities transported over large distances favor dense-phase transport [1].

Several technologies for dense-phase transport of hydrogen have been discussed in the literature. For instance, hydrogen can be stored in metal-organic frameworks [2], zeolites [3], as liquid organic hydrogen carriers [4,5], ammonia [6,7], or as liquefied hydrogen (LH_2) [8,9]. The arguably most promising candidate of these, both from a cost and energy point-of-view is LH_2, which gives superior flexibility in the receiving end with respect to purity, pressurization, aggregate state, distribution and usage [10]. The energy density of LH_2 is almost 4.5 times higher than that of compressed hydrogen at 200 bar [1,11]. This reduces the necessary volume and weight of transport and storage-facilities significantly.

So far, there has been no demand for large quantities of LH_2. As a consequence, the technology for liquefaction of hydrogen is still immature and inefficient. The exergy efficiency of existing liquefaction plants lies between 25% and 30% when factoring in the penalty for externally supplied liquid nitrogen for pre-cooling [12]. In currently operating hydrogen liquefaction plants, the specific energy requirement is 11.9 kWh/kg LH_2 for the Leuna plant [8], and slightly lower for newer plants. Several works have in recent years proposed novel solutions for lowering the energy requirements. The best process designs indicate that it is possible to reduce the energy demand below 6.0 kWh/kg LH_2 [8,13–16]. Further work on a more detailed level than overall process design is needed to realize this.

In a recent work [17], it was shown how the exergy destruction in the cryogenic heat exchangers of the hydrogen liquefaction process can be reduced by up to 43% by enhancing the activity of the catalyst and using a helium-neon mixture as refrigerant. In this work, we shall further explore the potential for improvement by optimally controlling the refrigerant temperature. Entropy production minimization [18] will be combined with optimal control theory [19] to study configurations with minimum entropy production. The aim of this work is two-fold: 1) To quantify the potential for improving the energy efficiency of the cryogenic heat exchangers by enhancing the thermal match between the cold and hot streams, 2) To obtain new insight into the characterization of process equipment with minimum entropy production.

Entropy production/generation minimization is a technique that has been exploited to gain insight into energy efficient design and operation of a wide range of examples in the literature such as heat exchangers [20–22], chemical reactors [23–26], distillation columns [27], thermal systems [28], refrigeration cycles [29] and many other processes [30–32]. Equipartition of the thermodynamic driving forces

and equipartition of the entropy production are principles that are often good approximations to systems with minimum entropy production. These principles can thus serve as practical guidelines for energy efficient design and operation [23,33]. For systems where the number of control variables equals the number of state variables, it has been shown [34] that minimum entropy production implies equipartition of the entropy production, which is equivalent with equipartition of the forces when the matrix of resistivities is constant. For most systems of practical relevance however, the number of control variables is lower than the number of state variables.

By examining thousands of numerical solutions of different plug flow reactor formulations [35], Johannessen and Kjelstrup found what they referred to as a "highway in state-space" that was particularly dense with solutions characterized by minimum entropy production. We will show and explain why the heat exchangers in the cryogenic part of the hydrogen liquefaction process do not follow highways in state-space and give new insight into the prerequisites for the appearance of the highway.

Theory

The system

In this work, a plate-fin heat exchanger in the cryogenic part of the hydrogen liquefaction process will be studied. Here, the hot layers are filled with catalyst to speed up the kinetics of the following spin-isomer reaction:

$$H_{2,o} \rightleftharpoons H_{2,p}, \qquad (1)$$

Where subscripts o and p refer to ortho and para hydrogen. With no catalyst, the heat that is generated when liquefied ortho-hydrogen converts to para-hydrogen in e.g. storage tanks will lead to full evaporation, since the enthalpy difference of ortho-para conversion exceeds the latent heat of evaporation at low temperatures.

In the plate-fin heat exchanger, cold and hot layers are placed in a repeating unit as illustrated in Figs. 1 and 2. If boundary effects are neglected, the behavior of the complete heat exchanger can be represented by considering only a repeating unit of hot and cold streams as shown in Fig. 1, which sequentially make up the full plate-fin heat exchanger that has $n = 2N$ number of layers in total, where N is the number of times the unit is repeated. Fins are included to increase the available heat transfer area as well as to induce turbulence to enhance the heat transfer. Two configurations will be studied in this work: A reference case where normal hydrogen is used as refrigerant and flows counter currently with the hot streams as illustrated in Fig. 2, and an optimization study where the temperature of the refrigerant, $T_a(z)$ can be controlled at every spatial position, z. The aim of the optimization study is to identify the temperature at the cold-side of the plate-fin heat exchanger that gives minimum entropy production/exergy destruction.
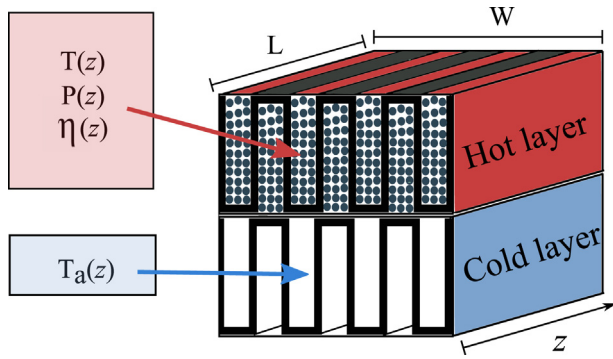
Fig. 1 – Illustration of the hot and cold layers in the plate-fin-heat exchanger and their governing variables. Fins are used in both layers to enhance the heat transfer coefficient and area, The hot layers are filled with catalyst and the cold layers are open.
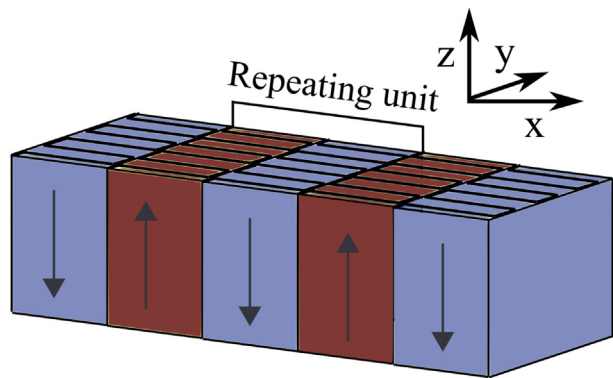

Fig. 2 – Illustration of the repeating unit and the counter current flows in the hot and cold layers in the plate-fin heat exchanger.

Balance equations for the catalyst filled layers

A plug-flow reactor formulation will be used to describe the layers of the heat exchanger. Here, the balance equations are area averaged in the direction perpendicular to the flow direction (in the x and y coordinates). The balance equations will be formulated for only two layers, where the number of layers, N will be used to scale up relevant quantities like local perimeter and flow rates to represent the full plate-fin heat exchanger. The spin-isomer conversion is taking place at the surfaces of the catalyst. To be able to compare to previous work [23,35] and to have a compact formulation, the conversion of the reaction is used as variable

$$\xi = \frac{\text{moles of ortho hydrogen consumed by the reaction}}{\text{moles of ortho hydrogen at inlet}}. \quad (2)$$

The flow rate of component i (ortho or para hydrogen) can then be obtain from:

$$F_i = F_i^0 + F_o^0 \nu \xi, \quad (3)$$

where superscript 0 refers to inlet conditions and ν is the stoichiometric vector of the reaction in Eq. (1). The mole fraction of component i is:

$$x_i = \frac{F_i}{F_o + F_p}. \quad (4)$$

The mass balance of the hot layers can be expressed in terms of the conversion of the reaction as

$$\frac{d\xi}{dz} = \frac{\Omega}{F_o^0} r. \quad (5)$$

Here, r is the rate of the reaction defined in Eq. (1), Ω the cross sectional area and z is the spatial coordinate in the direction of the flow. The expression for the reaction rate of the ortho-to para-hydrogen spin conversion was taken from Ref. [17]. The layers with ortho- and para-hydrogen were described as an ideal mixture between ortho and para-hydrogen at local equilibrium at each position z, where the multiparameter equation of state by Leachman et al. [11] was used to describe the thermodynamic properties of ortho and para hydrogen. The energy balance of a hot layer is formulated in terms of a differential equation for the temperature:

$$\frac{dT}{dz} = \frac{PJ_q + \Omega[r(-\Delta_r H)] - \left(\frac{\partial H}{\partial P}\right)_{T,F_i} \frac{dP}{dz}}{\sum_{i=1}^n F_i C_{p,i}}. \quad (6)$$

Here P is the perimeter of one layer of the heat exchanger, $C_{p,i}$ is the specific heat of component i, $\Delta_r H$ is the enthalpy of the reaction, H is the total enthalpy and P is the pressure. The *momentum balance* equation relates the pressure drop (dP/dz) to the fluid velocity (v). For a fully developed flow through a packed bed, the pressure drop can be modeled by Hicks equation [36]:

$$\frac{dP}{dz} = -f \rho v^2 / D_p, \quad (7)$$

Where D_p is the diameter of the catalyst pellets, ρ is the mass density, v is the velocity and and f is the friction factor. The friction factor is given by

$$f = 6.8 \frac{(1-\varepsilon)^{1.2}}{\varepsilon^3 Re_p^{0.2}}. \quad (8)$$

Here $Re_p = D_p v \rho / \mu$, where μ is the viscosity of the fluid and ε is the catalyst bed void fraction. The density was found from information about the temperature, pressure and composition by using a density solver in combination with the equation of state [37,38].

Balance equations for the cold layer and the heat flux

In the reference case, we will use standard hydrogen as refrigerant. The cold layers are open (not filled with catalyst) and refrigerant flows counter-currently with the fluid in the hot layers as illustrated in Fig. 2. We used the following equation to represent the temperature of the cold layer (subscript a):

$$\frac{dT_a}{dz} = \frac{-PJ_q}{\sum_{i=1}^{n} F_{a,i}^0 C_{p,i,a}} \tag{9}$$

Where we neglected the pressure drop in the open layers, as it does not contribute significantly to the total entropy production of the plate-fin heat exchanger, as discussed in Ref. [17]. The heat flux is calculated with reference to the perimeter of the hot layers:

$$J_q = U(T_a - T), \tag{10}$$

where the overall heat transfer coefficient, U, was in the reference case computed by using state-of-the-art correlations for a plate-fin-heat exchanger described in detail in previous work [17].

In the optimization procedure, T_a was allowed to change, and to be able to compare to the reference case, it was assumed that the heat transfer properties were the same. Therefore, a constant value, U equal to the spatial mean of the overall heat transfer coefficient from the complete model described in Ref. [17], $\widehat{U}$ was used in the optimization:

$$U = \frac{1}{L} \int_0^L \widehat{U}[T(z), P(z), \eta(z), T_a(z)]dz, \tag{11}$$

Where L is the total length of the heat exchanger (see Fig. 1) and the overall heat transfer coefficient of the complete model depended on the state variables both in the hot (T, P, η) and cold layers (T_a).

The entropy production and the lost work

The lost work in the plate-fin heat exchanger is connected to the total entropy production through the Gouy-Stodola theorem [18].

$$w_{\text{lost}} = w - w_{\text{ideal}} = T_0 \left(\frac{dS}{dt}\right)_{\text{irr}}. \tag{12}$$

Here T_0 is the temperature of the environment, w is the work, w_{ideal} is the work needed or consumed in an ideal, reversible process and $\left(\frac{dS}{dt}\right)_{\text{irr}}$ is the total entropy production. Johannessen showed in his thesis [39] that maximizing the lost work was equivalent to minimizing the total entropy production if the inlet and outlet states of the reactor were fixed. In this work, we shall minimize the total entropy production as it is the true source of irreversibility in the process unit as shown by Eq. (12). For the cases studied in this work, the total entropy production is the integral of the local entropy production:

$$\left(\frac{dS}{dt}\right)_{\text{irr}} = \int_0^L \sigma(z)dz \tag{13}$$

where the local entropy production of the unit can be derived by use of nonequilibrium thermodynamics [40]. The framework of nonequilibrium thermodynamics has successfully giving insight into a variety of examples ranging from thermoelectric generators [41] to ion-exchange membranes [42] and gas-liquid interfaces [43]. The local entropy

production of the repeating unit illustrated in Fig. 1 becomes:

$$\sigma = PJ_q \left(\frac{1}{T} - \frac{1}{T_a}\right) + \Omega v \left(-\frac{1}{T}\frac{dP}{dz}\right) + \Omega r_{o \to p} \left(-\frac{\Delta G_r}{T}\right) \tag{14}$$

Where ΔG_r is Gibbs free energy of the spin isomer reaction.

The optimization problem and optimal control theory

In this work, we will find the state of minimum total entropy production:

$$\min \left(\frac{dS}{dt}\right)_{\text{irr}} \tag{15}$$

Where the objective function depends on the *state variables* T, P, ξ that are constrained by the balance equations in Eqs. (5)–(7) and the *control variable* T_a that is allowed to vary freely. We refer to Ref. [39] for an excellent introduction to optimal control theory for reactor system. The procedure in optimal control theory is to define the Hamiltonian, which for this example becomes:

$$H = \sigma + \lambda_T \frac{dT}{dz} + \lambda_P \frac{dP}{dz} + \lambda_\xi \frac{d\xi}{dz} \tag{16}$$

Where λ_T, λ_P and λ_ξ are Lagrange multiplier functions. Optimal control theory gives the following differential equations that define the necessary conditions for a minimum:

$$\frac{dT}{dz} = \frac{\partial H}{\partial \lambda_T} \qquad \frac{d\lambda_T}{dz} = -\frac{\partial H}{\partial T} \tag{17}$$

$$\frac{dP}{dz} = \frac{\partial H}{\partial \lambda_P} \qquad \frac{d\lambda_P}{dz} = -\frac{\partial H}{\partial P} \tag{18}$$

$$\frac{d\xi}{dz} = \frac{\partial H}{\partial \lambda_\xi} \qquad \frac{d\lambda_\xi}{dz} = -\frac{\partial H}{\partial \xi}, \tag{19}$$

and an algebraic equation for the control variable:

$$\frac{\partial H}{\partial T_a} = 0. \tag{20}$$

The Hamiltonian of this optimal control problem is autonomous, meaning that it has only an implicit dependence on the spatial coordinate, z, through the state variables, the control variables or the Lagrange multiplier functions. For such problems, the Hamiltonian is constant along the z-coordinate. In order to complete the optimal control problem, we have to specify the boundary conditions for the state variables, i.e. the inlet and outlet values of T, P and ξ. We shall fix the boundary conditions for some of these variables, and use free boundary conditions for others. When the boundary conditions for state variables are free to vary, the corresponding Lagrange multiplier is zero at the same spatial position [39].

Equipartition principles

In this work, we shall evaluate two design principles that have been used in the literature to approximate the state of minimum entropy production, equipartition of forces (EoF) and equipartition of the entropy production (EoEP). Eq. (14) shows that there are three thermodynamic driving forces in the

process unit considered in this work; the thermal driving force, the pressure drop and the driving force for the spin isomer reaction. EoF can only be realized for the thermal driving force since T_a is the only control variable. With EoF, $T_a(z)$ is controlled to satisfy boundary values for relevant state variables and the following criterion:

$$\frac{d}{dz}\left(\frac{1}{T(z)} - \frac{1}{T_a(z)}\right) = 0, \qquad (21)$$

Which defines equipartition of the thermal driving force. With EoEP, $T_a(z)$ is controlled to satisfy boundary values for relevant state variables and the following criterion:

$$\frac{d\sigma(z)}{dz} = 0, \qquad (22)$$

Which defines equipartition of the entropy production for the example considered in this work. The constant value of the thermal driving force or the local entropy production has to be adjusted to match boundary conditions from the reference case. Since there is only one variable to adjust, but several relevant state-variables at the outlet, we shall consider two variants of EoEP and EoF.

EoEP-T and EoF-T: The constant value of the local entropy production or the thermal driving force is adjusted to match the outlet temperature of the reference case, T^L.

EoEP-x and EoF-x: The constant value of the local entropy production or the thermal driving force is adjusted to match the outlet mole-fraction of para hydrogen from the reference case, x_p^L.

Cases and computational details

The reference cases

In the reference cases, we consider a plate-fin heat exchanger in the bottom part of hydrogen liquefaction process where the exergy destruction is largest. Catalyst filled plate-fin exchangers are state-of-the-art technology due to their high area-to-volume-ratio and capability to continuously convert ortho-hydrogen to para-hydrogen [16].

The heat exchanger studied in this work is one of several heat exchangers in a Claude refrigeration cycle with a production capacity of 50 tons of liquid hydrogen per day. A sketch of the layout of such a process is presented in Fig. 1 in Ref. [16]. The purpose of the heat exchanger is to cool the reacting hydrogen where catalyst is present from 47.8 K to a target temperature for the reacting hydrogen of 29.3 K. The cold-side refrigerant inlet temperature is 28.9 K. Before final expansion, the reacting hydrogen stream is very close to the Joule–Thomson inversion line. The refrigerant stream in this case is gaseous hydrogen expanded through cryo-expanders. Most of the inlet conditions to the heat exchanger can be found in Table 2. The geometrical specifications of the plate-fin heat exchanger were discussed in detail in previous work [17], and similar parameters are used here as summarized in Table 1, where the meaning of the parameters is shown in Fig. 3.

In a recent work by Donaubauer et al. [44], they discuss the effect of elevating the operation pressure, where the display benefits of raising the operation pressure from 25 bar to 75 bar.

Table 1 – The geometry of the plate-fin heat exchanger for the reference cases.

Parameter	Value
Length (L)	1 m
Height (H)	0.8 m
Width (W)	1.5 m
Fin height (b)	$4 \cdot 10^{-3}$ m
Fin thickness (t)	$3.5 \cdot 10^{-4}$ m
Fin spacing (s)	$1.1 \cdot 10^{-3}$ m
Parting sheet distance	$1.5 \cdot 10^{-3}$ m
Number of repeating units	68

Table 2 – The common inlet conditions (superscript 0) for the two reference cases.

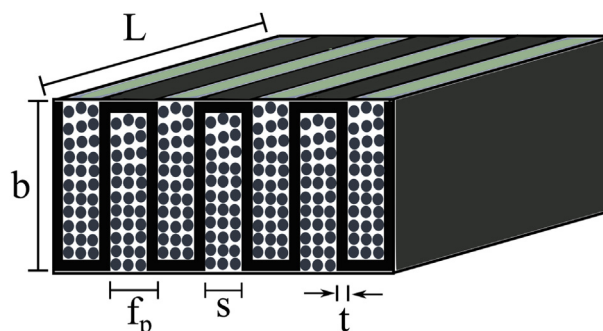| Parameter	Value
T^0	47.8 K
T_a^0	28.9 K
P_a^0	5.0 bar
x_p^0	0.767
$x_{p,a}^0$	0.25

Fig. 3 – The geometrical variables that define the layers of the plate-fin heat exchanger. Their values for the reference cases are provided in Table 1.

The benefit of raising the operation pressure has also been discussed previously by Cardella et al. [16]. In light of recent discussions, we study in this work two reference cases; one where the feed stream enters at 20 bar, and one where it enters at 80 bar. The only differences between these cases are the inlet pressure of the feed stream and the flow rate of refrigerant presented in Table 3. In the reference cases, the overall heat transfer coefficient was determined by using the state-of-the-art empirical correlations presented in Ref. [17]. They varied through the heat exchanger due to a change in the state variables. The temperature and conversion of ortho-hydrogen at the inlet/outlet, and the mean heat transfer coefficient from the reference cases as computed by Eq. (11) were used as input parameters in the optimization study.

Computing states with minimum entropy production

The same strategy as in previous work [39] was used to identify the state of minimum entropy production. First, a

Par	20-bar case	80-bar case
P^0	20 bar	80 bar
F_a^0	14.7 mol/s	8.8 mol/s
U	347 W/m²K	219 W/m²K

numerical optimization routine was carried out on a relatively coarse grid (30 points) with the Matlab 9.2-routine *fmincon*, where the discretized balance equations and suitable boundary conditions were used. The profiles that minimized the total entropy production numerically were used to create an initial guess for the optimal control problem. The boundary value problem from optimal control theory was then solved by using the collocation method, *bvp4c* in Matlab. The combination of numerical and analytical optimization was very robust. The agreement between the results from the numerical optimization and optimal control theory strengthen the assumption that a global minimum has indeed been identified.

Results and discussion

A comparison of the 20- and 80-bar cases

The 20- and 80-bar reference cases were solved to a relative accuracy of 10^{-6}. The resulting temperature and composition profiles are shown in Figs. 4 and 5 (thick solid lines). The corresponding profiles that give minimum entropy production with the same boundary conditions have also been included for comparison (thin dashed lines). The optimal profiles lie below the reference through most of the heat exchanger for the 20-bar case, while the opposite can be seen for the 80-bar case.

Table 4 reveals that there is a potential to reduce the total entropy production by 8.7% and 4.3% in the 20- and 80-bar cases. The table also shows that the total entropy production of the 80-bar reference case is about 25% lower than that of the 20-bar reference case. This indicates that an inlet pressure of 80-bar gives a more efficient operation of the heat exchanger than 20 bar, as discussed in the literature [8,13—16]. However, it is misleading to only compare the total entropy production of these cases, since also the duty of the heat exchangers are very different. A total of 0.366 MW of heat is
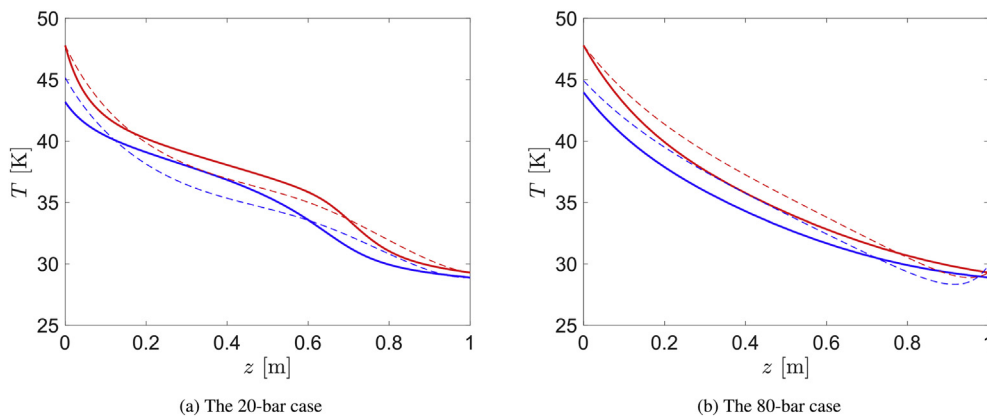
(a) The 20-bar case

(b) The 80-bar case

Fig. 4 — The temperatures in the hot (red) and cold (blue) layers of the heat exchanger for the reference case (thick solid lines) and the case with minimum entropy production (thin dashed lines) for the 20-bar case (left) and the 80-bar case (right)

(a) The 20-bar case

(b) The 80-bar case

Fig. 5 — The mole fraction of para hydrogen in the hot layers (lower red) and the mole fraction of para hydrogen at equilibrium (upper blue) for the reference case (thick solid lines) and the case with minimum entropy production (thin dashed lines) for the 20-bar case (left) and the 80-bar case (right)
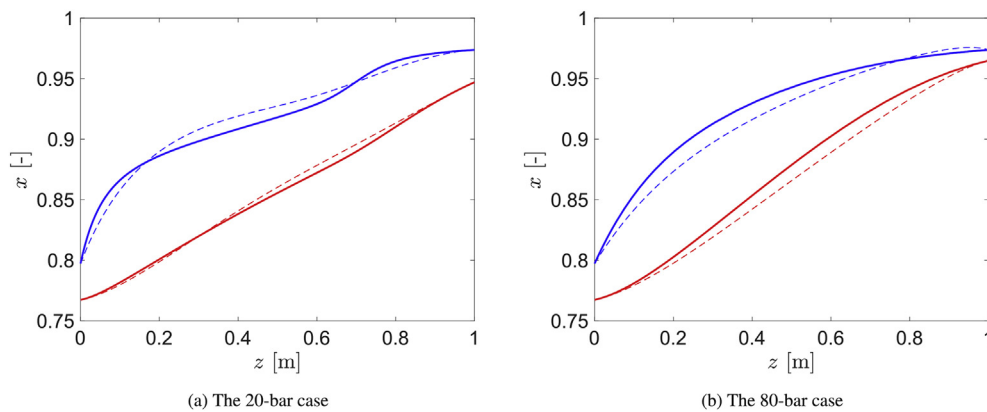
Cases	P_0 [bar]	T^L [K]	x_p^L	$(dS/dT)_{\mathrm{irr}}$ [J/Ks]	$(dS/dT)_{\mathrm{irr}}^{\min}$ [J/Ks]	Change
Ref.	20	**29.30**	**0.947**	11.70	10.67	−8.74%
EoEP-T	20	**29.30**	0.939	9.82	9.80	−0.18%
EoEP-x	20	28.02	**0.947**	10.99	10.97	−0.16%
EoF-T	20	**29.30**	0.942	10.09	10.07	−0.18%
EoF-x	20	28.45	**0.947**	10.85	10.84	−0.14%
Ref.	80	**29.30**	**0.965**	8.85	8.46	−4.33%
EoEP-T	80	**29.30**	0.952	7.10	7.09	−0.12%
EoEP-x	80	27.39	**0.965**	8.61	8.60	−0.14%
EoF-T	80	**29.30**	0.956	7.44	7.42	−0.32%
EoF-x	80	28.07	**0.965**	8.50	8.46	−0.47%

Table 4 – Key results from the cases investigated. Boundary conditions that are the same as in the reference cases are highlighted in bold.

transferred between the hot and cold layers in the 20-bar case, while only 0.230 MW is transferred in the 80-bar case. The difference between these duties must be compensated for when compressing the hydrogen from 20 to 80 bar.

Furthermore, the overall heat transfer coefficient is approximately 60% higher in the 20-bar case than in the 80-bar case as shown in Table 3, which favors a lower thermal entropy production and a higher efficiency. Unfortunately, there is a thermal mismatch in the 20-bar case at a position of $z \approx 0.6$ m which is the source of most of the entropy production, as discussed in detail in Ref. [17]. The origin of this thermal mismatch is the large increase in the heat capacity of the hydrogen in the hot layer due to the supercritical conditions, as shown in Fig. 6. This increase in the heat capacity is also visible in the temperature difference between the hot and cold layers in the 20-bar reference case, which displays an increase around $z = 0.6$ m.

If the difference in duty is also taken into account, the two reference cases perform similarly. By following the procedure outlined in Ref. [39], it is possible to compute the second law efficiency for the two reference cases, η_{II}, which gives $\eta_{II} = 0.91$ for the 20-bar case and $\eta_{II} = 0.89$ for the 80-bar case, i.e. a very similar performance. In the work by Donaubauer et al. [44],

they show that a higher operating pressure results in a lower outlet temperature and a higher ortho-to-para conversion rate for *a fixed* refrigerant flow rate. We observe the same behavior in our study. However, even though a higher refrigerant flowrate in the 80-bar case gives a higher overall heat transfer coefficient, we find that it also gives a larger thermal mismatch at the inlet of the heat exchanger. If the same refrigerant flow rate is used in the 80-bar Case as in the 20-bar Case, this nearly doubles the total entropy production due to large thermal mismatch at the inlet.

Whether it is beneficial to carry-out the cryogenic refrigeration of the hydrogen at 20 or 80 bars of pressure depends therefore on how efficiently the gas can be compressed and whether it pays off to trade the entropy production in the heat exchangers with the corresponding entropy production in the compressors. A typical exergy efficiency of compressors in combination with intercoolers in the hydrogen liquefaction process is 0.7 [12]. Therefore, it is most likely not beneficial to target a high pressure in the heat exchangers in the hydrogen liquefaction process. A detailed evaluation of the overall process is necessary to give further insight into this.

The use of equipartition as design principle for the heat exchangers of the hydrogen liquefaction process

We shall next discuss whether Equipartition of the Entropy Production (EoEP) or Equipartition of Forces (EoF) can be used as principles to achieve energy efficient design or operation of the heat exchangers in the hydrogen liquefaction process. A comparison of the local entropy production profiles in of the reference cases (solid lines), with those that give minimum entropy production (dashed lines) shows that the latter appear to have less variations through the heat exchanger. Clearly, the profiles that give minimum entropy production are not perfectly constant, such as those with EoEP (red dash-dot lines).

In the optimization problem considered in this work, there was only one control variable, the temperature of the refrigerant, $T_a(z)$. Of this reason, EoEP and and EoF were unable to simultaneously match the outlet temperature, T^L and mole fraction of para hydrogen, x_p^L. The large entropy production associated with the ortho-para hydrogen conversion is reflected in a high sensitivity with respect to boundary conditions, where the total entropy production from EoEP differs by more than 10% depending on whether the outlet temperature
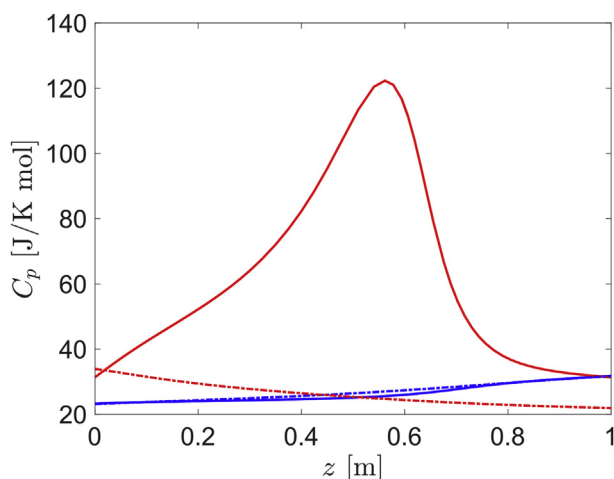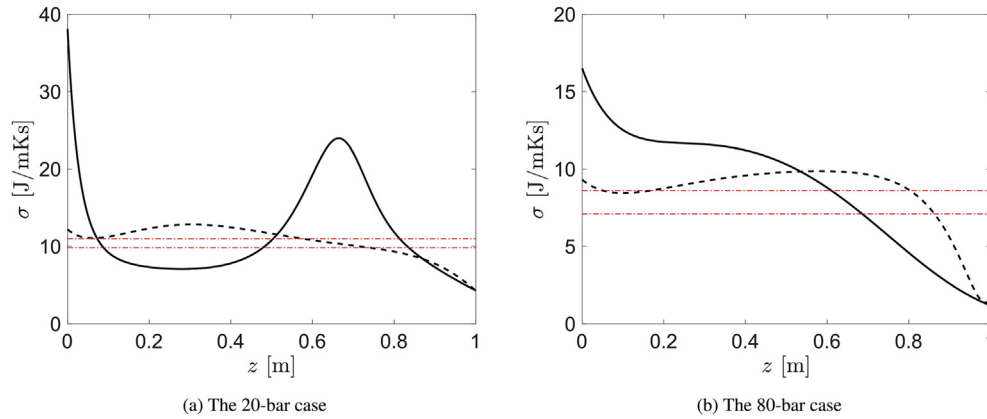

Fig. 6 – The heat capacity in the cold (blue) and the hot (red) layers of the heat exchanger in the 20-bar case (solid lines) and 80-bar case (dash-dot lines). (For interpretation of the references to colour in this figure legend, the reader is referred to the Web version of this article.)

(a) The 20-bar case

(b) The 80-bar case

Fig. 7 — The local entropy production for the repeating unit of the reference case (thick solid lines), the case with minimum entropy production (thin dashed lines), the EoEP-cases where the outlet mole fraction of para-hydrogen (upper dash-dot lines) or the outlet temperature (lower dash-dot lines) are the same as in the reference case, for the 20-bar case (left) and the 80-bar case (right)

(EoEP-T) or the outlet mole fraction (EoEP-x) are used as boundary conditions. The value of the local entropy production in EoEP with the two different boundary conditions is shown by the dash-dot lines in Fig. 7, where there is a clear distinction between the upper and lower lines. The same is true for EoF, where only the thermal force can be controlled directly. This prevents a direct comparison of the total entropy production from the reference cases and the EoEP and EoF solutions, since the outlet state of the hot layer becomes significantly different from the reference cases as shown in the third and fourth columns of Table 4.

A more coherent way to compare the performance of the reference cases and the EoEP and EoF solutions is to compare the relative improvement with respect to a state of minimum entropy production where the same boundary conditions are imposed. The sixth column of Table 4 presents the total entropy production for an optimally controlled heat exchanger that has the exact same outlet temperature and composition as the respective cases, as stated by columns three and four. Column seven shows the

relative improvement in percentage that is possible by optimally controlling the refrigerant temperature. The table reveals that the total entropy productions from EoEP and EoF deviate only 0.2% and 0.5% from the state of minimum entropy production. Of these two, EoF gives outlet states that are most similar to the reference cases. The present analysis indicates that for all practical purposes, a constant thermal driving force $(1/T - 1/T_a)$ represents a simple guideline that should be targeted in the design and operation of heat exchangers in the cryogenic part of the hydrogen liquefaction process. This guideline could be used in practice both when determining the geometrical specifications of the heat exchanger, as well as in determining process design parameters such as pressure-levels and distribution of the heat exchangers.

Disappearance of the highway in state-space

Johannessen and Kjelstrup presented in 2005 what they referred to as a "highway in state-space" that was particularly

(a) Normal reaction rate
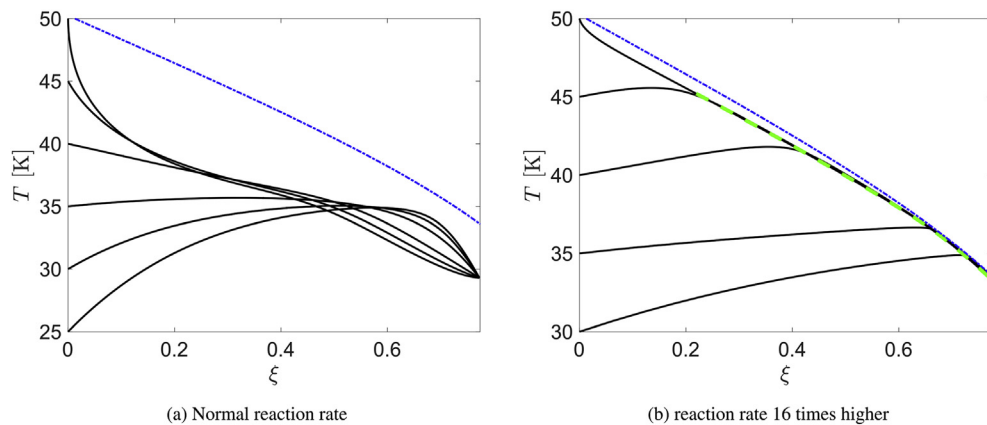
(b) reaction rate 16 times higher

Fig. 8 — Solutions with minimum entropy production with input parameters from the reference case and different inlet temperatures (left) and the same cases with the reaction rate multiplied by 16 (right). The blue dash-dot lines correspond to the equilibrium conversion at a given temperature. (For interpretation of the references to colour in this figure legend, the reader is referred to the Web version of this article.)

dense with solutions characterized by minimum entropy production [35]. The highway emerged as a narrow band when the interior temperature of the reactor was plotted as a function of the degree of reaction, even with widely different boundary conditions. The reactors were characterized by a "reaction mode" off the highway, where chemical reactions dominated the entropy production, and a "heat transfer mode" along the highway, where the thermal entropy production dominated.

Fig. 8 shows the temperature of the hot layers as a function of the degree of reaction for several inlet temperatures for the process unit considered in this work, where all profiles give minimum entropy production with their respective boundary conditions. In difference to previous reactors studied in the literature, the process unit considered on this work does not follow the dense band referred to as the highway in state space.

The reason for this is that the spin-isomer conversion of ortho to para hydrogen is too slow to give a "reaction mode" at the inlet of the process unit, and the spin-isomer reaction contributes therefore significantly to the total entropy production throughout the whole process unit. By artificially increasing the reaction rate, the highway in state-space (green dashed line) appears when the reaction rate becomes sufficiently high as shown in Fig. 8b. Here, the reaction rate has been artificially increased by 16 times. The temperature through the process unit is much closer to the equilibrium temperature (blue dash-dot line) in Fig. 8b than in Fig. 8a. These results indicate that a prerequisite for a process unit to have a highway in state-space, is that it exhibits a reaction mode at the inlet followed by a heat transfer mode, where the heat transfer mode is a results of the mixture being sufficiently close to chemical equilibrium through most of the length of the process unit.

Conclusion

In this work, we have studied a plate-fin heat exchanger in the cryogenic part of the hydrogen liquefaction process that cools the hydrogen from 47.8 K to 29.3 K. The heat exchanger is also a reactor, since catalyst is placed in the hot layers to speed up the highly exothermic conversion of ortho-to para-hydrogen.

By combining entropy generation minimization with optimal control theory, we studied heat exchanger configurations with minimum entropy production/exergy destruction. The objective function was the total entropy production, the control variable was the temperature of the refrigerant in the cold layers and the constrains were the balance equations for energy, mass and momentum in the hot layers.

Two reference cases were studied; one where the feed stream entered at 20 bar, and one where it entered at 80 bar. The main argument for a higher operation pressure is that a thermal mismatch between the hot and cold layers at 20 bar can be avoided. This mismatch stems from a peak in the heat capacity of the fluid in the hot layers.

By using the same overall heat transfer coefficient as in the reference cases, we found that the optimal refrigeration strategies gave a reduction of the total entropy production by 8.7% in the 20-bar case and 4.3% in the 80-bar case. The overall

heat transfer coefficient and duty was higher in the 20 bar case, which compensated for the increase in entropy production from the thermal mismatch. The second law efficiency of the 20 bar Case (91%) was therefore similar to the 80 bar Case (89%). Hence, it is likely better to choose an operation pressure of 20 bar, since the efficiency of the heat exchangers is similar, but the exergy destruction associated with the additional compression is avoided.

The refrigerant temperature was further adjusted to obtain Equipartition of the Entropy Production (EoEP) or Equipartition of the thermal driving Force (EoF) to approximate the state of minimum entropy production. Since there was only one control variable, but two relevant outlet boundary conditions, we found that EoEP and EoF were unable to match the outlet boundary conditions of the reference cases, which prevented a direct comparison. However, by considering the state of minimum entropy production constrained by the exact same boundary conditions as those from EoEP or EoF, we found that they yielded total entropy productions that deviated less than 0.2% and 0.5% from the minimum. Equipartition of the thermal driving force i.e. the difference between the inverse temperatures of the hot and cold layers is a particularly straightforward guideline that is recommended for this process unit.

Recent literature has shown that the interior temperature of plug flow reactor formulations with minimum entropy production follow a narrow band when plotted as a function of the degree of reaction, even with widely different boundary conditions. This band has been referred to as the "highway". We found that the process unit considered in this work did not give a highway in state-space. The reason was that both heat transfer and reaction contributed significantly to the total entropy production throughout its length. In difference to previous examples in the literature, the process unit could not be characterized by a "reaction mode" (off the highway) at the inlet followed by a "heat transfer mode" (at the highway). We found that the highway appeared after the reaction rate had been artificially increased to a sufficient degree, such that the hot layers were significantly closer to chemical equilibrium through the process unit. This indicates that a prerequisite for a process unit to have a highway is that it has a reaction mode at the inlet followed by a heat transfer mode.

REFERENCES

[1] Burheim OS. Engineering energy storage. London, United Kingdom: Elsevier; 2017.

[2] Li J, Cheng S, Zhao Q, Long P, Dong J. Synthesis and hydrogen-storage behavior of metal—organic framework MOF-5. Int J Hydrogen Energy 2009;34(3):1377—82. https://doi.org/10.1016/j.ijhydene.2008.11.048.

[3] Dong J, Wang X, Xu H, Zhao Q, Li J. Hydrogen storage in several microporous zeolites. Int J Hydrogen Energy 2007;32(18):4998—5004. https://doi.org/10.1016/j.ijhydene.2007.08.009.

[4] Preuster P, Papp C, Wasserscheid P. Liquid organic hydrogen carriers (LOHCs): toward a hydrogen-free hydrogen economy. Acc Chem Res 2017;50(1):74—85. https://doi.org/10.1021/acs.accounts.6b00474.

[5] Shi L, Qi S, Qu J, Che T, Yi C, Yang B. Integration of hydrogenation and dehydrogenation based on dibenzyltoluene as liquid organic hydrogen energy carrier. Int J Hydrogen Energy 2019;44:5345—54. https://doi.org/10.1016/j.ijhydene.2018.09.083.

[6] Klerke A, Christensen CH, Nørskov JK, Vegge T. Ammonia for hydrogen storage: challenges and opportunities. J Mater Chem 2008;18:2304—10. https://doi.org/10.1039/B720020J.

[7] Lamb KE, Dolan MD, Kennedy DF. Ammonia for hydrogen storage; A review of catalytic ammonia decomposition and hydrogen separation and purification. Int J Hydrogen Energy 2019;44:3580—93. https://doi.org/10.1016/j.ijhydene.2018.12.024.

[8] Berstad DO, Stang JH, Nekså P. Large-scale hydrogen liquefier utilizing mixed-refrigerant pre-cooling. Int J Hydrogen Energy 2010;35(10):4512—23. https://doi.org/10.1016/j.ijhydene.2010.02.001.

[9] Garceau NM, Baik JH, Lim CM, Kim SY, Oh I-H, Karng SW. Development of a small-scale hydrogen liquefaction system. Int J Hydrogen Energy 2019;40:11872—8. https://doi.org/10.1016/j.ijhydene.2015.06.135.

[10] Bauer A, Mayer T, Semmel M, Morales MAG, Wind J. Energetic evaluation of hydrogen refueling stations with liquid or gaseous stored hydrogen. Int J Hydrogen Energy 2019;44:6795—812. https://doi.org/10.1016/j.ijhydene.2019.01.087.

[11] Leachman JW, Jacobsen RT, Penoncello SG, Lemmon EW. Fundamental equations of state for parahydrogen, normal hydrogen, and orthohydrogen. J Phys Chem Ref Data 2009;38:721. https://doi.org/10.1063/1.3160306.

[12] Berstad DO, Stang JH, Nekså P. Comparison criteria for large-scale hydrogen liquefaction processes. Int J Hydrogen Energy 2009;34(3):1560—8. https://doi.org/10.1016/j.ijhydene.2008.11.058.

[13] Quack H. Conceptual design of a high efficiency large capacity hydrogen liquefier. AIP Conf Proc 2002;613:255. https://doi.org/10.1063/1.1472029.

[14] Valenti G, Macchi E. Proposal of an innovative, high-efficiency, large-scale hydrogen liquefier. Int J Hydrogen Energy 2008;33:3116—21. https://doi.org/10.1016/j.ijhydene.2008.03.044.

[15] Report on technology overview and barriers to energy- and cost-efficient large scale hydrogen liquefaction. FCH JU FP7-JTI Project. IDEALHY Consortium; 2012. Tech. Rep. Ref. 278177 D1.1.

[16] Cardella U, Decker L, Klein H. Economically viable large-scale hydrogen liquefaction. IOP conference series: materials science and engineering, vol. 171; 2017. p. 012012. https://doi.org/10.1088/1757-899X/171/1/012013.

[17] Wilhelmsen Ø, Berstad D, Aasen A, Nekså P, Skaugen G. Reducing the exergy destruction in the cryogenic heat exchangers of hydrogen liquefaction processes. Int J Hydrogen Energy 2018;43(10):5033—47. https://doi.org/10.1016/j.ijhydene.2018.01.094.

[18] Bejan A. Entropy generation minimization: the method of thermodynamic optimization of finite-size systems and finite-time processes. New York: CRC Press; 1996.

[19] Troutman JL. Variational calculus and optimal control: optimization with elementary convexity. Berlin: Springer; 1995.

[20] Guo J, Cheng L, Xu M. Optimization design of shell-and-tube heat exchanger by entropy generation minimization and genetic algorithm. Appl Therm Eng 2009;29(14—15):2954—60. https://doi.org/10.1016/j.applthermaleng.2009.03.011.

[21] Babaelahi M, Sadri S, Sayyaadi H. Multi-objective optimization of a cross-flow plate heat exchanger using entropy generation minimization. Chem Eng Technol 2014;37(1):87—94. https://doi.org/10.1002/ceat.201300411.

[22] Xie G, Song Y, Asadi M, Lorenzini G. Optimization of pin-fins for a heat exchanger by entropy generation minimization and constructal law. J Heat Transf 2015;137(6):061901. https://doi.org/10.1115/1.4029851.

[23] Johannessen E, Kjelstrup S. Minimum entropy production rate in plug flow reactors: an optimal control problem solved for SO_2 oxidation. Energy 2004;29(12—15):2403—23. https://doi.org/10.1016/J.ENERGY.2004.03.033.

[24] Wilhelmsen Ø, Johannessen E, Kjelstrup S. Energy efficient reactor design simplified by second law analysis. Int J Hydrogen Energy 2010;35(24):13219—31. https://doi.org/10.1016/j.ijhydene.2010.08.118.

[25] Wang C, Chen L, Xia S, Sun F. Maximum production rate optimization for sulphuric acid decomposition process in tubular plug-flow reactor. Energy 2016;99:152—8. https://doi.org/10.1016/J.ENERGY.2016.01.040.

[26] Chen L, Zhang L, Xia S, Sun F. Entropy generation minimization for CO_2 hydrogenation to light olefins. Energy 2018;147:187—96. https://doi.org/10.1016/J.ENERGY.2018.01.050.

[27] Mullins OC, Stephen Berry R. Minimization of entropy production in distillation. J Phys Chem 1984;88:723—8. https://doi.org/10.1021/j150648a022.

[28] Durmayaz A, Sogut OS, Sahin B, Yavuz H. Optimization of thermal systems based on finite-time thermodynamics and thermoeconomics. Prog Energy Combust Sci 2004;30(2):175—217. https://doi.org/10.1016/J.PECS.2003.10.003.

[29] le Roux WG, Bello-Ochende T, Meyer JP. Thermodynamic optimisation of the integrated design of a small-scale solar thermal Brayton cycle. Int J Energy Res 2012;36(11):1088—104. https://doi.org/10.1002/er.1859.

[30] Sciacovelli A, Verda V, Sciubba E. Entropy generation analysis as a design tool—a review. Renew Sustain Energy Rev 2015;43:1167—81. https://doi.org/10.1016/J.RSER.2014.11.104.

[31] Magnanelli E, Wilhelmsen Ø, Acquarone M, Folkow L, Kjelstrup S. The nasal geometry of the reindeer gives energy-efficient respiration. J Non-Equilib Thermodyn 2017;42(1):59—78. https://doi.org/10.1515/jnet-2016-0038.

[32] Magnanelli E, Wilhelmsen Ø, Johannessen E, Kjelstrup S. Energy efficient design of membrane processes by use of entropy production minimization. Comput Chem Eng 2018;117:105—16. https://doi.org/10.1016/J.COMPCHEMENG.2018.06.002.

[33] Thiel GP, McGovern RK, Zubair SM, Lienhard V JH. Thermodynamic equipartition for increased second law efficiency. Appl Energy 2014;118:292—9. https://doi.org/10.1016/J.APENERGY.2013.12.033.

[34] Johannessen E, Kjelstrup S. Nonlinear flux-force relations and equipartition theorems for the state of minimum entropy production. J Non-Equilib Thermodyn 2005;30(2):129—36. https://doi.org/10.1515/JNETDY.2005.009.

[35] Johannessen E, Kjelstrup S. A highway in state space for reactors with minimum entropy production. Chem Eng Sci

2005;60(12):3347–61. https://doi.org/10.1016/J.CES.2005.01.026.

[36] Hicks RE. Pressure drop in packed beds of spheres. Ind Eng Chem Fundam 1970;9(3):500–2. https://doi.org/10.1021/i160035a032.

[37] Wilhelmsen Ø, Skaugen G, Hammer M, Wahl PE, Morud JC. Time efficient solution of phase equilibria in dynamic and distributed systems with differential algebraic equation solvers. Ind Eng Chem Res 2013;52:2130–40. https://doi.org/10.1021/ie302579w.

[38] Wilhelmsen Ø, Aasen A, Skaugen G, Aursand P, Austegard A, Aursand E, Gjennestad M, Lund H, Linga G, Hammer M. Thermodynamic modeling with equations of state: present challenges with established methods. Ind Eng Chem Res 2017;56(13):3503–15. https://doi.org/10.1021/acs.iecr.7b00317.

[39] Johannessen E. The state of minimum entropy production in an optimally controlled system. Norwegian University of Science and Technology; 2004. PhD. thesis.

[40] Kjelstrup S, Bedeaux D. Non-equilibrium thermodynamics of heterogeneous systems. World Scientific; 2008.

[41] Børset MT, Wilhelmsen Ø, Kjelstrup S, Burheim OS. Exploring the potential for waste heat recovery during metal casting with thermoelectric generators: on-site experiments and mathematical modeling. Energy 2017;118:865–75. https://doi.org/10.1016/J.ENERGY.2016.10.109.

[42] Zlotorowicz A, Strand RV, Burheim OS, Wilhelmsen Ø, Kjelstrup S. The permselectivity and water transference number of ion exchange membranes in reverse electrodialysis. J Membr Sci 2017;523:302–408. https://doi.org/10.1016/j.memsci.2016.10.003.

[43] Wilhelmsen Ø, Trinh TT, Lervik A, Badam VK, Kjelstrup S, Bedeaux D. Coherent description of transport across the water interface: from nanodroplets to climate models. Phys Rev 2016;93(3):032801. https://doi.org/10.1103/PhysRevE.93.032801.

[44] Donaubauer PJ, Cardella U, Decker L, Klein H. Kinetics and heat exchanger design for catalytic ortho-para hydrogen conversion during liquefaction. Chem Eng Technol 2019;42:669–79.